Manufacture of Passive Dynamic Ankle–Foot Orthoses Using Selective Laser Sintering

Mario C. Faustini, Richard R. Neptune*, Richard H. Crawford, and Steven J. Stanhope

***Abstract*—Ankle–foot orthosis (AFO) designs vary in size, shape, and functional characteristics depending on the desired clinical application. Passive Dynamic (PD) Response ankle–foot orthoses (PD-AFOs) constitute a design that seeks to improve walking ability for persons with various neuromuscular disorders by passively (like a spring) providing variable levels of support during the stance phase of gait. Current PD-AFO manufacturing technology is either labor intensive or not well suited for the detailed refinement of PD-AFO bending stiffness characteristics. The primary objective of this study was to explore the feasibility of using a rapid freeform prototyping technique, selective laser sintering (SLS), as a PD-AFO manufacturing process. Feasibility was determined by replicating the shape and functional characteristics of a carbon fiber AFO (CF-AFO). The study showed that a SLS-based framework is ideally suited for this application. A second objective was to determine the optimal SLS material for PD-AFOs to store and release elastic energy; considering minimizing energy dissipation through internal friction is a desired material characteristic. This study compared the mechanical damping of the CF-AFO to PD-AFOs manufactured by SLS using three different materials. Mechanical damping evaluation ranked the materials as Rilsan™ D80 (best), followed by DuraForm™ PA and DuraForm™ GF. In addition, Rilsan™ D80 was the only SLS material able to withstand large deformations.**

***Index Terms*—Design automation, freeform fabrication, orthotics.**

I. Introduction

ANKLE–FOOT orthoses (AFOs) are devices often prescribed to improve gait performance for persons with impaired lower limb function as assistive or therapeutic devices. For the purpose of this study, the classification *active dynamic* orthosis contains those devices that use motors [1], pumps [2], and actuators [3] to actively control the magnitude of joint assistance and level of mechanical energy transferred.

Manuscript received February 28, 2007. The opinions presented in this paper reflect the views of the authors and not those of the National Institutes of Health or the U.S. Public Health Service. The research activities conducted at The University of Texas at Austin were supported in part by a contract from the Physical Disabilities Branch, National Institutes of Health. *Asterisk indicates corresponding author.*

M. C. Faustini and R. H. Crawford are with the Department of Mechanical Engineering, The University of Texas at Austin, Austin, TX 78712-0292 USA (e-mail: faustini@alumni.utexas.net; rhc@mail.utexas.edu).

*R. R. Neptune is with the Department of Mechanical Engineering, The University of Texas at Austin, Austin, TX 78712-0292 USA (e-mail: rneptune@mail.utexas.edu).

S. J. Stanhope is with the Physical Disabilities Branch, National Institutes of Health, Bethesda, MD 20892-1604 USA (e-mail: steven_stanhope@nih.gov).

Color versions of one or more of the figures in this paper are available online at http://ieeexplore.ieee.org.

Digital Object Identifier 10.1109/TBME.2007.912638

Fig. 1. Carbon fiber AFO design (Dynamic Brace, Advanced Prosthetics and Orthotics Inc., Jacksonville, FL).

The classification *passive dynamic* (PD) orthosis contains AFO designs that rely on characteristics such as material properties, component thickness [4], AFO shape [5]–[7], springs [8], and fluid pressure dynamics [9], [10], to establish bending or rotational stiffness characteristics and to regulate the storage and return of mechanical energy. While many clinical reasons exist for the prescription of rigid AFOs, one functional goal of contemporary PD-AFOs is to achieve smooth efficient walking by providing a variable level of support and mechanical energy return to the ankle during stance in gait [11], [12].

In recent studies, PD-AFOs containing carbon fiber (CF) composite have been shown to increase walking speed and overall gait performance in patients with post-polio syndrome [11], stroke [13] and cerebral palsy [4]. Of the various CF-AFO designs, the Dynamic Brace (Dynamic Bracing Solutions, Inc., San Diego, CA) is a passive dynamic response AFO well-suited as a test case for this project since it is made entirely of continuous carbon composite, is readily scalable, and uses material properties and alterations in component dimensions to establish rotational stiffness (Fig. 1). In addition, its design is well-suited for determining a value for rotational stiffness that is appropriate for gait [14].

Manufacture of CF-AFOs is a multi-step process requiring a substantial level of highly skilled labor [15]. While methods to automate AFO shape customization using parameterization have been proposed [16], such methods have been limited by the lack of automated manufacturing methods. A promising engineering solution for producing customized PD-AFOs is the application of selective laser sintering (SLS) technology [17],

which is a versatile manufacturing technique that provides several advantages over traditional methods and has been successfully used to fabricate prosthetic sockets for lower limb amputees [18]–[22]. SLS is a manufacturing technique that fabricates any closed solid model in sequential cross-sectional layers. A planar layer of a powdery material is placed in the part bed and melted or sintered in the desired cross-section of the model, which is then allowed to solidify. The bed is then lowered by one layer thickness and covered again with another layer of the powdery material and the process is repeated. When all the cross-sections of the model are processed, the final part possesses the same shape and dimensions as the computer model. Thus, SLS allows the manufacture of PD-AFOs directly from digital shape information of the patient's limb, which eliminates the necessity for preliminary molds, hand lamination and finishing procedures. Also, SLS can create complex geometric features with no cost penalty in manufacturing, which significantly expands the options for developing and exploring new PD-AFO designs and optimizing their characteristics (e.g., weight and stiffness). In addition, SLS uses a computer-modeling environment compatible with finite element method (FEM) tools for pre-manufacturing analyses to assess structural integrity and mechanical performance. Hence, the primary objective of this study was to explore the feasibility of using a SLS-based design, analysis and manufacturing framework to rapidly produce patient-specific PD-AFOs.

A second objective was to identify the most appropriate SLS material for manufacturing PD-AFOs. Patients with various neuromuscular disorders often lose control and strength in their lower limbs, which impairs their mobility. The storage and release of elastic energy within the structure of a PD-AFO is an important design characteristic that helps compensate for various neuromuscular disorders. For example, during the second rocker phase of stance in gait the PD-AFO deforms under the influence of the body weight, thus storing elastic energy. Following heel off in stance the AFO becomes unloaded. During this third rocker phase of stance in gait, the AFO releases the stored energy to help satisfy the energetic demands of walking. Thus, a fundamental criterion for selecting the most appropriate SLS material for AFO fabrication is minimizing energy dissipation through internal friction during AFO deformation. The present study evaluated the energy dissipation characteristics in three nylon-based SLS materials: DuraForm™ PA (Nylon 12), DuraForm™ GF (glass-filled Nylon 12) and Rilsan™ D80 (Nylon 11). These material characteristics were then compared to those of the Dynamic Brace CF-AFO.

II. Methods

A. PD-AFO Design and Manufacturing Framework

To facilitate a direct comparison of the damping properties between the SLS fabricated AFOs and the Dynamic Brace CF-AFO, a SLS design and manufacturing framework was developed to replicate the geometry and design characteristics of the CF-AFO. The framework included the following steps (Fig. 2): 1) determining the bending stiffness of the CF-AFO; 2) developing a surface model of the CF-AFO; 3) developing a computer-aided design (CAD) model of the CF-AFO from the surface model; 4) performing a FEM analysis of the CAD model using anticipated load conditions; 5) iteratively modifying the digital AFO strut dimensions to reproduce the stiffness and structural characteristics of the CF-AFO; and 6) using SLS to fabricate three working prototypes, each manufactured using one of three materials (DuraForm™ PA (PA-AFO), DuraForm™ GF (GF-AFO), and Rilsan™ D80 (D80-AFO) using SLS. The SLS fabrication system used in this study was a 3D Systems (Valencia, CA) Vanguard HS Sinterstation. Each of these steps is described in detail below.

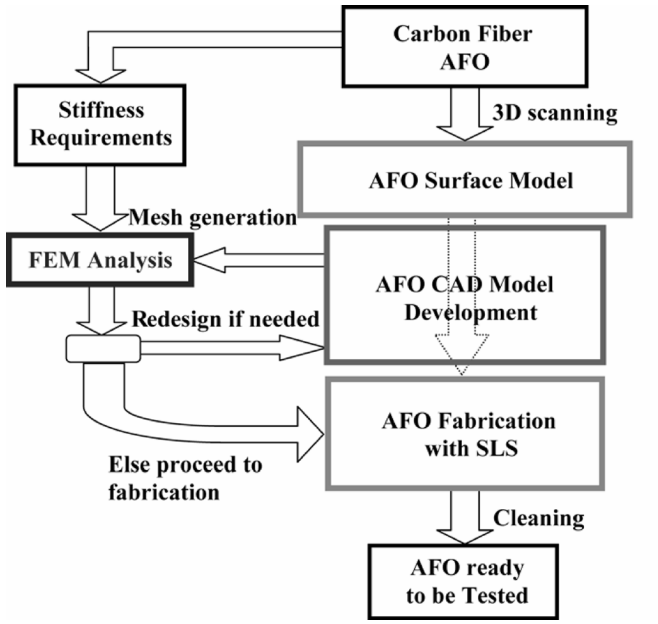

Fig. 2. Framework for the AFO design and SLS fabrication to duplicate the CF-AFO design characteristics.

B. Surface Model Development

The CF-AFO used in this study [Fig. 3(a)] was obtained with the consent of a 66-year-old male subject (height 1.85 m, weight 81.8 kg) with Post-Polio Syndrome who was prescribed and routinely wore bilateral CF-AFOs for enhanced gait performance. The subject provided his written consent to participate in this Institutional Review Board approved study.

Computed tomography (CT) images of the CF-AFO alone were acquired using a CT scanner (LightSpeed QX/i, GE Medical Systems). The CF-AFO was placed on a slight angle to maximize surface area in the imaging plane. Images were acquired in helical mode using a 1.25 mm slice thickness and 0.98 mm in-plane pixel resolution yielding an array of $512 \times 512 \times 431$ pixels. A cloud of points delineating the surface of the AFO was extracted using the custom-written National Institutes of Health (NIH) software, Medical Image Processing Analysis and Visualization (MIPAV). A custom-written program was then used to convert the pixel coordinates into real coordinates (millimeters) and save them in VRML97 format. This format was then triangularized [Fig. 3(b)] and decimated by Raindrop Geomagic™ (Raindrop Geomagic, Inc, Research Triangle Park, NC) software [Fig. 3(c)].

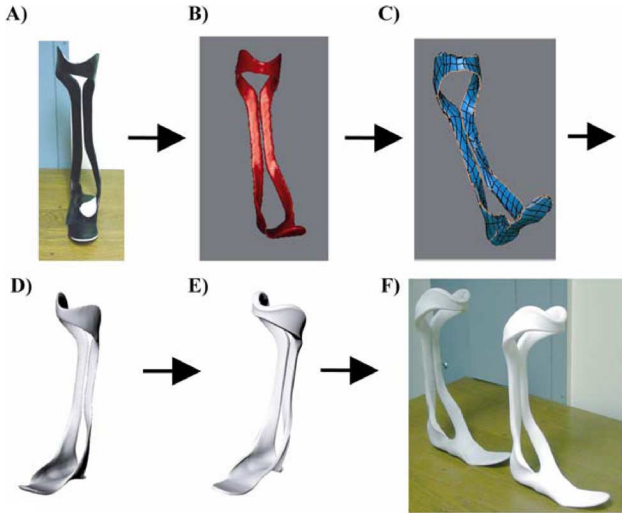

Fig. 3. Steps for modeling and fabrication of SLS AFOs to be tested from original carbon fiber AFO. (a) Original carbon fiber AFO design (Dynamic Brace, Advanced Prosthetics and Orthotics Inc., Jacksonville, FL) to be replicated with SLS. (b) Corresponding point cloud file from the digitized AFO. (c) Reconstructed point cloud. (d) Surface model. (e) Solid model. (f) SLS manufactured AFO prototypes.

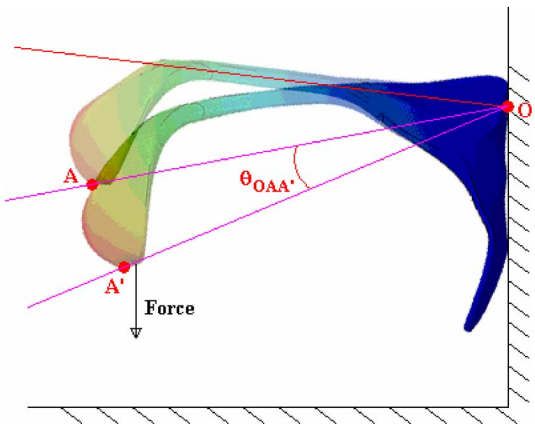

Fig. 4. Rotational stiffness of the AFO in the sagittal (viewing) plane, defined as the ratio between the applied normal force and the resulting deformation angle $\theta_{OAA'}$.

C. AFO Computer-Aided Design (CAD) Model Development

The resulting CF-AFO model was then converted to a CAD model and subsequent designs were finalized using Rhinoceros™ 3D (Seattle, WA) software [Fig. 3(d)]. Three models were created from this file, one for each of the SLS materials to be tested. Each solid model [Fig. 3(e)] preserved the overall geometric characteristics of the CF-AFO. However, the cuff width and strut length were decreased such that the standing height of the AFO was decreased 15% in order to fit within the build volume of the SLS workstation. In addition, the thickness of the struts in each model was modified to assure the AFO's rotational stiffness (an important functional characteristic) in the sagittal plane (Fig. 4) matched that of the CF-AFO, which was verified through FEM analyses and physical testing (both described below).

TABLE I
MATERIAL PROPERTIES FOR THE SLS MATERIALS

Property	Rilsan D80	DuraForm PA	DuraForm GF
Tensile strength	45 MPa	44 MPa	38.1 MPa
Tensile modulus	1400 MPa	1600 MPa	5910 MPa
Flexural modulus	869 MPa	1285 MPa	3300 MPa
Tensile elongation at break	25%	9%	2%

D. FEM Analysis

FEM software (EDS I-deas™, Plano, TX) was used for iterative analysis to determine the cross-sectional strut dimensions of the SLS manufactured AFOs. The CF-AFO CAD model was imported into I-deas™ using the IGES file format. A Delaunay-based [23] mesh generator was used to create the initial model mesh using 10-node parabolic tetrahedral elements. The initial element size was chosen in the mesh generator to be smaller than the overall AFO thickness for both the cuff and footplate. The automated mesh generator was set to create a model based on sections, allowing specific areas and geometric features to be further refined. The resulting mesh was then interactively inspected to identify highly distorted or stretched elements that might lead to errors in the analysis. When such areas were identified, individual elements were locally refined. The complete FEM mesh for the AFO had a total of 13 345 elements and 24 235 nodes. The material properties used in the FEM analysis are provided in Table I.

E. Load Conditions

The FEM analysis for the AFO models was performed under typical able-bodied gait loading and boundary conditions in order to evaluate the flexural response of the AFO, which would assure the SLS manufactured AFO rotational stiffness matched the CF-AFO. If the resulting value was found to be too high or too low, the cross sectional areas (thicknesses) of the two struts were adjusted accordingly and a new simulation was performed. The iterative process continued until the desired rotational stiffness was achieved. The loading model consisted of an inbound surface force applied to the faces of the elements that shared the frontal inner surface of the cuff, replicating the force applied by the shank of the leg on the AFO cuff during walking. The bottom of the footplate was spatially restrained.

F. SLS Fabrication of AFOs

The files were then converted to STL format and AFOs were fabricated in a 3DSystems Vanguard HS Sinterstation using DuraForm™ PA, DuraForm™ GF and Rilsan™ D80 material. Since the modeled AFOs were 17.7 inches tall, each AFO occupied the entire 18-inch build volume (due to the build height space lost to extra warm up and cool down powder layers) and had to be positioned diagonally to fit within the build boundaries of the SLS workstation. This orientation was, however, consistent across all AFO builds. Each build took approximately 26 hours, including warming-up and cooling-down stages. An additional 6 hours were necessary, after finishing the build, for the part bed temperature to drop below 50 °C and

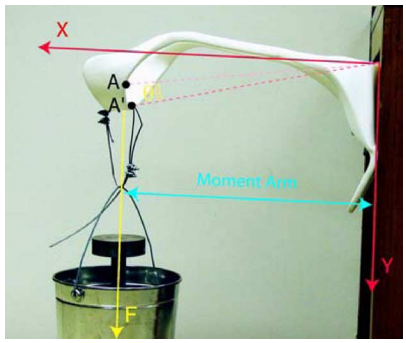

Fig. 5. The experimental testing of the rotational stiffness was performed by clamping the footplate and applying an increasing force F at the cuff, then measuring the resulting angle θ created by the deformation of the AFO in relation to its resting position.

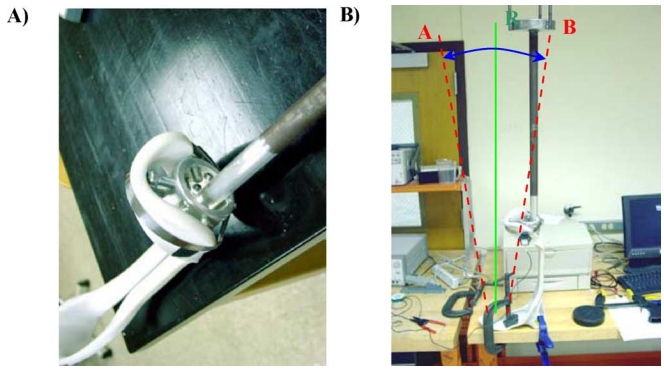

Fig. 6. Energy dissipation measurement set up. (a) Detail of attachment between testing rod and cuff of AFO. (b) Diagram of experiment, testing rod was brought from resting point R to initial point A and then released, and then allowed to oscillate freely between points A and B as mechanical damping dissipated energy and the system returned to resting point R.

allow safe removal of the AFOs. The part bed was broken out, and the AFO was then cleaned with a sandblaster in preparation for testing [Fig. 3(f)]. Thus the construction of each AFO took approximately 32 hours from start to finish. Note that SLS workstation runs automatically without human intervention during the build cycle. Although up to two AFOs could be built simultaneously in the SLS system using the same material feed, each AFO was built independently in this study.

G. Experimental Tests and FEM Validation

Experimental analyses were performed on the AFO prototypes to compare the structural response of the AFOs with the FEM predictions and identify the mechanical limits of the SLS AFOs. Using similar boundary conditions, nondestructive tests were set up to evaluate bending stiffness. The experimental test procedure (Fig. 5) consisted of clamping the footplate of the AFO against a vertical base and applying an increasing vertical force to the cuff through a system of cables and masses. For each increase of 45 N in applied force, the angle between the location of the uppermost point at the front of the cuff in this deformed state and its original location in the AFO's resting state was recorded. The force was increased to 490 N, and then decreased to zero while the same angle was measured. With this moment versus angular displacement data, the rotational stiffness could be readily determined and used to validate the FEM results.

H. Measuring Energy Dissipation

The energy dissipation measurement for all four AFOs (i.e., the original CF-AFO and the three SLS prototypes) consisted of securely attaching to the cuff of each AFO a long iron rod, which had a lumped mass at the distal end [Fig. 6(a)] to produce a rigid AFO-rod system. The iron rod was 800 mm tall and weighed 9 kg (including the distal lumped mass). Each AFO was then fixed on a table and a calibrated accelerometer (Crossbow CXL04P3) was attached to the side of the cuff and connected to a data acquisition system [Fig. 6(b)]. The AFO was rotated 20 degrees in the sagittal plane and released. Accelerometer data were collected during the following 30 seconds. Five measurement trials were performed for each AFO.

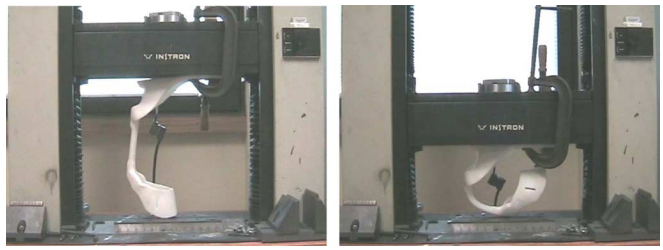

Fig. 7. Destructive test where a compressive load was applied to a SLS AFO, forcing it to bend to its maximum limits.

From the resulting acceleration-time trajectory, energy dissipation was quantified by the decay factor d of the best-fit envelope curve Ae^{-dt}, where t is time. The initial 5 seconds of acquired data were discarded to allow small out-of-plane vibrations to subside and the oscillations to reach steady-state. For each AFO, d was averaged over the five measurement trials.

I. Destructive Tests

Destructive tests were performed to evaluate the AFOs' ultimate flexural strength using a hydraulic axial load cell (MTS Systems Corp., Eden Prairie, MN). In these tests, the SLS AFOs were loaded through the full range of motion while positioned between the crosshead and the base of the load cell. This forced the struts to fold while the cuff was pushed by the base of the testing machine towards the footplate, which was clamped against the crosshead (Fig. 7).

III. Results

The proposed framework proved to be a feasible process to generate AFOs directly from the scanned image data, with the design characteristics being nearly identical to the CF-AFO. Table II lists physical characteristics of the SLS and CF- AFOs.

A. Energy Dissipation in AFOs

The energy dissipation data (Fig. 8) for the CF-AFO showed a decay factor of $d = 0.0488$, which was the lowest amount of energy dissipation of the four AFOs tested. DuraForm™ GF had

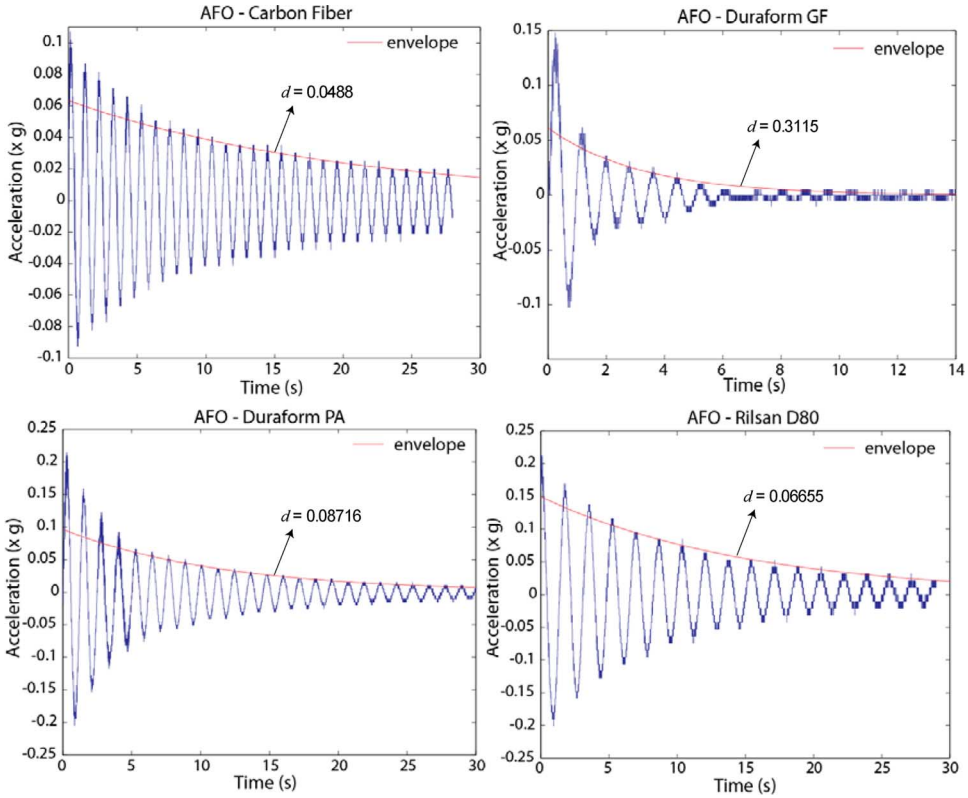

Fig. 8. For each tested AFO, values of acceleration (times gravity acceleration) versus time (in seconds) were plotted and the best-fit envelope curve for which the decay factor d was calculated.

TABLE II
PHYSICAL CHARACTERISTICS OF THE AFOS

Property\AFO Material	Rilsan D80	DuraForm PA	DuraForm GF	Carbon Fiber
Weight (g)	575	349	478	598
Cross sectional area of each strut (mm^2)	581	485	352	*179
Standing height (mm)	444	444	444	525
Distal toe plate to inferior cuff edge (mm)	385	385	385	443
Heel to distal toe on footplate (mm)	238	238	238	293

*Average cross sectional area of the two carbon fiber struts

TABLE III
AFO ROTATIONAL STIFFNESS

Property\AFO Material	Rilsan D80	DuraForm PA	DuraForm GF	Carbon Fiber
Rotational stiffness (N-m/degree)	10.18	10.47	11.03	10.69

the largest energy dissipation, with $d = 0.3115$. DuraForm™ PA had a decay factor $d = 0.08716$, while Rilsan™ D80 had a $d = 0.06655$, which was the lowest amount of dissipation among the SLS fabricated AFOs. In all four cases, deviations in the averaged d values were similar and less than 5%.

B. Mechanical Properties of AFOs

The mechanical characteristics of the SLS AFOs were considered satisfactory with a rotational stiffness within 5% of the FEM designed target stiffness values (Table III), thus successfully validating the framework's FEM predictions. However, the destructive tests showed that only Rilsan™ D80 was able to withstand large deformations without failing, although some permanent plastic deformation was observed. Both DuraForm™ PA and DuraForm™ GF fractured during the destructive test.

IV. DISCUSSION

The primary objective of this study was to explore the feasibility of using an SLS-based manufacturing framework to produce patient-specific PD-AFOs. A second objective was to identify the most appropriate SLS material to be used for manufacturing the AFOs. Using the proposed framework, three SLS AFOs were fabricated with different materials and evaluated relative to the functional characteristics of a commercially available CF-AFO. Rilsan™ D80 proved to be the SLS material that exhibited the least amount of energy dissipation through mechanical damping and was the only material to withstand the destructive testing.

Mechanical damping characteristics ranked the SLS materials as Rilsan™ D80 (best), followed by DuraForm™ PA and DuraForm™ GF (worst). However, mechanical damping in the Rilsan™ D80 AFO was still significantly higher (36%) than the CF-AFO, which may influence patient fatigue during

long-term AFO use. Since minimizing damping in a PD-AFO is an important characteristic, future work should be directed at optimizing the SLS-based PD-AFO design itself (e.g., using topology optimization) to minimize energy losses. However, although different PD-AFO designs could lead to a decrease in energy losses, the ranking of mechanical damping characteristics should remain similar among the materials analyzed. Another aspect that could alter the mechanical damping is the part orientation during the SLS fabrication. Since the SLS process is a layer based process, and even within the layer plane the material is not expected to be perfectly uniform due to the prevalent laser scan direction, a change in the part orientation alone could be enough to modify internal friction in the SLS PD-AFOs. Thus, future work should also be directed towards identifying the influence of build orientation on the mechanical damping characteristics of SLS PD-AFOs.

A potential limitation of the current SLS framework is the maximum build envelop, which is intrinsic to commercially available SLS fabrication systems and limits the height of AFOs. Future work should focus on developing alternative AFO designs that are not constrained by the build envelop, such as two-part designs that can be readily assembled after fabrication.

Another important area of future work is to assess the effect of dynamic and impulsive loading conditions on the structural integrity and durability of the SLS PD-AFOs. While such loading conditions are not primary considerations for clinical reasons, active patients using these AFOs are likely to encounter situations that will require resistance to dynamic loads. Assessment of these load cases will require additional destructive and nondestructive experimentation and the determination of the fatigue properties of the SLS materials. Impact resistance of the SLS PD-AFOs was preliminarily tested with mixed results. The prototypes were dropped from a height of 1.0 meter and none failed, but some fractured when dropped from 2.3 meters. A more controlled investigation of impact resistance is warranted.

The present study used an existing CF-AFO design to allow direct comparison of the damping characteristics of SLS fabricated AFOs with the commercially available yet extensively customized CF-AFO. However, one of the primary advantages of the present framework is that it allows for systematic and controlled design modifications in the AFO shape or volume, which permits the exploration of the relative advantages of various PD-AFO designs (e.g., alternative strut designs to achieve different rotational stiffness values, as illustrated in Fig. 9) and the ability to make subject-specific PD-AFOs. To produce a subject-specific PD-AFO, existing designs can be simply scaled to a scanned image of the patient's limb and the framework applied to optimize the PD-AFO design characteristics to satisfy a clinician's prescription to suit a patient's specific needs [Fig. 9(a)]. For example, in the present study the rotational stiffness was fine-tuned to match the CF-AFO with the FEM tools by simply scaling the cross-sectional areas of the struts (Table II). Such customization could be extended to assist clinicians in meeting each patient's specific needs. A second advantage is that additional features such as holes for strapping around the cuff and attachment features for motion capture systems for clinical analyses [Fig. 9(b)] can be easily integrated into an AFO design.

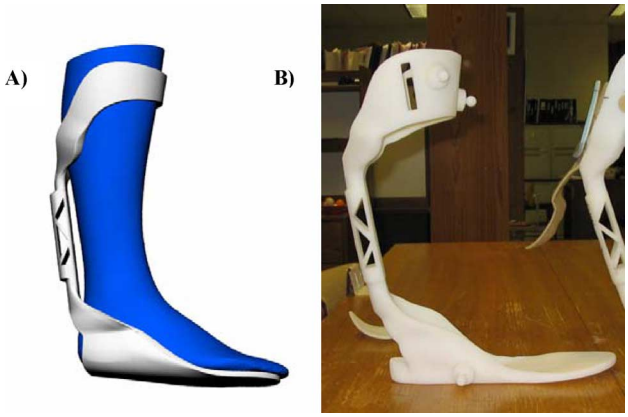

Fig. 9. (a) Alternative design with single strut AFO designed using topology optimization tools [24] and (b) additional features added for straps and motion capture markers.

With the present framework, modifying the design to optimize and improve a clinician's ability to enhance patient performance can be achieved and structurally analyzed before the PD-AFO is manufactured to ensure a structurally sound design and provide long-term reliability. Thus, the presented SLS design, analysis and manufacture framework exhibits considerable promise for fabricating AFOs customized for specific patients.

REFERENCES

[1] J. M. Hidler and A. E. Wall, "Alterations in muscle activation patterns during robotic-assisted walking," *Clin. Biomech.*, vol. 20, pp. 184–93, Feb. 2005.

[2] K. E. Gordon, G. S. Sawicki, and D. P. Ferris, "Mechanical performance of artificial pneumatic muscles to power an ankle-foot orthosis," *J. Biomech.*, vol. 39, pp. 1832–41, 2006.

[3] J. A. Blaya and H. Herr, "Adaptive control of a variable-impedance ankle-foot orthosis to assist drop-foot gait," *IEEE Trans. Neural Syst. Rehabil. Eng.*, vol. 12, no. 1, pp. 24–31, Mar. 2004.

[4] A. Bartonek, M. Eriksson, and E. M. Gutierrez-Farewik, "A new carbon fibre spring orthosis for children with plantar flexor weakness," *Gait Posture*, vol. 25, pp. 652–6, Apr. 2007.

[5] R. E. Major, P. J. Hewart, and A. M. MacDonald, "A new structural concept in moulded fixed ankle foot orthoses and comparison of the bending stiffness of four constructions," *Prosthet. Orthot. Int.*, vol. 28, pp. 44–8, Apr. 2004.

[6] T. Sumiya, Y. Suzuki, and T. Kasahara, "Stiffness control in posterior-type plastic ankle-foot orthoses: Effect of ankle trimline. Part 2: Orthosis characteristics and orthosis/patient matching," *Prosthet. Orthot. Int.*, vol. 20, pp. 132–7, Aug. 1996.

[7] T. Sumiya, Y. Suzuki, and T. Kasahara, "Stiffness control in posterior-type plastic ankle-foot orthoses: Effect of ankle trimline. Part 1: A device for measuring ankle moment," *Prosthet. Orthot. Int.*, vol. 20, pp. 129–31, Aug. 1996.

[8] S. Yamamoto, M. Ebina, T. Kubo, T. Hayashi, Y. Akita, and Y. Hayakawa, "Development of an ankle-foot orthosis with dorsiflexion assist, part 2: Structure and evaluation," *J. Prosthet. Orthot.*, vol. 9, pp. 1–9, 1999.

[9] S. Yamamoto, A. Hagiwara, T. Mizobe, O. Yokoyama, and T. Yasui, "Development of an ankle-foot orthosis with an oil damper," *Prosthet. Orthot. Int.*, vol. 29, pp. 209–19, Dec. 2005.

[10] O. Yokoyama, H. Sashika, A. Hagiwara, S. Yamamoto, and T. Yasui, "Kinematic effects on gait of a newly designed ankle-foot orthosis with oil damper resistance: A case series of 2 patients with hemiplegia," *Arch. Phys. Med. Rehabil.*, vol. 86, pp. 162–6, Jan. 2005.

[11] L. S. Halstead, D. T. Crittenden, J. P. Nielsen, and M. Loke, "Dynamic bracing: A novel approach to lower extremity bracing for individuals with incomplete spinal cord injury and other neuromuscular disorders," *J. Spinal Cord Med.*, vol. 26, p. S16, 2003.

[12] S. Yamamoto, M. Ebina, S. Miyazaki, H. Kawai, and T. Kubota, "International forum: Development of a new ankle-foot orthosis with dorsiflexion assist, part 1: Desirable characteristics of ankle-foot orthoses for hemiplegic patients," *Arch. Phys. Rehabil.*, vol. 9, pp. 1–7, 1997.
[13] A. Danielsson and K. S. Sunnerhagen, "Energy expenditure in stroke subjects walking with a carbon composite ankle foot orthosis," *J. Rehabil. Med.*, vol. 36, pp. 165–8, Jul. 2004.
[14] K. M. Nelson, T. M. Kepple, K. L. Siegel, L. S. Halstead, and S. J. Stanhope, "Ankle foot orthosis contribution to net ankle moments in gait," in *Proc. Amer. Soc. Biomech.*, Toledo, OH, 2003.
[15] S. Hale, "Carbon fiber articulated AFO — An alternative design," *J. Prosthet. Orthot.*, vol. 1, pp. 191–195, 1989.
[16] A. L. Darling and W. Sun, "Orthotic design through 3D reconstruction: A passive-assistance ankle-foot orthotic," *Appl. Bion. Biomech.*, vol. 1, pp. 93–99, 2006.
[17] J. J. Beaman, J. W. Barlow, D. L. Bourell, R. H. Crawford, H. L. Marcus, and K. P. McAlea, *Solid Freeform Fabrication: A New Direction in Manufacturing*. Boston, MA: Kluwer, 1997.
[18] M. C. Faustini, R. H. Crawford, R. R. Neptune, W. E. Rogers, and G. Bosker, "Design and analysis of orthogonally compliant features for local contact pressure relief in transtibial prostheses," *J. Biomech. Eng.*, vol. 127, pp. 946–51, Nov. 2005.
[19] M. C. Faustini, R. R. Neptune, R. H. Crawford, W. E. Rogers, and G. Bosker, "An experimental and theoretical framework for manufacturing prosthetic sockets for transtibial amputees," *IEEE Trans. Neural Syst. Rehabil. Eng.*, vol. 14, no. 3, pp. 304–10, Sep. 2006.
[20] D. Freeman and L. Wontorcik, "Stereolithography and prosthetic test socket manufacture: A cost/benefit analysis," *J. Prosthet. Orthot.*, vol. 10, 1998.
[21] W. E. Rogers, A. Gitter, G. Bosker, M. C. Faustini, M. Lockhande, and R. H. Crawford, "Clinical evaluation of prosthetic sockets manufactured by selective laser sintering," presented at the 2001 Solid Freeform Fabrication Symp., Austin, TX, 2001.
[22] N. E. Walsh, J. L. Lancaster, V. W. Faulkner, and W. E. Rogers, "A computerized system to manufacture prostheses for amputees in developing countries," *J. Prosthet. Orthot.*, vol. 1, pp. 165–181, 1989.
[23] S. G. Zachariah and J. E. Sanders, "Interface mechanics in lower-limb external prosthetics: A review of finite element models," *IEEE Trans. Rehabil. Eng.*, vol. 4, pp. 288–302, Dec. 1996.
[24] M. P. Bendsoe and O. Sigmund, "Material interpolation schemes in topology optimization," *Arch. Appl. Mechan.*, vol. 69, pp. 635–657, 1999.

Mario C. Faustini received the B.S. degree in mechatronics engineering and the M.S.M.E. degree from the University of São Paulo, São Paulo, Brazil, in 1997 and 1999, respectively, and the Ph.D. degree from The University of Texas at Austin in 2004.

From 2004 to 2006, he was a Postdoctoral Fellow at The University of Texas at Austin. He is currently a consultant in Brazil. His research interests include development and application of computational tools in the design, analysis and simulation of prosthetics and orthotics, rehabilitation engineering and the application of solid freeform fabrication techniques such as selective laser sintering.

Richard R. Neptune received the B.S., M.S., and Ph.D. degrees in mechanical engineering from the University of California at Davis in 1991, 1993, and 1996, respectively.

He completed a Postdoctoral Fellowship at the University of Calgary, Canada, from 1996 to 1998. He then served as a Biomedical Engineer at the VA Palo Alto Rehabilitation Research and Development Center, Palo Alto, CA, from 1998 to 2000. He is currently an Associate Professor with the Department of Mechanical Engineering, The University of Texas at Austin. His research interests include musculoskeletal modeling and simulation of human movement, prosthetic and orthotic design optimization, rehabilitation and neuromotor control of movement.

Richard H. Crawford received the B.S.M.E. degree from Louisiana State University, Baton Rouge, in 1982, and the M.S.M.E. and Ph.D. degrees from Purdue University, West Lafayette, IN, in 1985 and 1989, respectively.

He is currently a Professor with the Department of Mechanical Engineering, The University of Texas at Austin. His research interests include development of computational representations and tools to support exploration of complex engineering design spaces and geometric processing, design tools, and manufacturing applications of solid freeform fabrication techniques such as selective laser sintering.

Steven J. Stanhope received the B.S. degree from Boston University, Boston, MA, in 1980, and the M.A. degree in biomechanics and exercise physiology and Ph.D. degree in biomechanics, human anatomy and exercise physiology from the University of Maryland at College Park in 1983 and 1985, respectively.

Between 1985 and 2001, he developed and directed the Biomechanics Laboratory in the Warren Grant Magnuson Clinical Center at the National Institutes of Health (NIH), Bethesda, MD. Since 2001, he has served as Director of the Physical Disabilities Branch at the NIH. His personal research interests include the development and implementation of novel instrumentation and biomechanically-based modeling and analysis techniques for rehabilitation and disability research.

Dr. Stanhope is a founding member of the Gait and Clinical Movement Analysis (GCMA) Society and of the Italian Society of Clinical Movement Analysis. He maintains memberships in the American Society of Biomechanics (ASB), the International Society of Biomechanics (ISB) and the SIAMOC. He maintains adjunct faculty appointments in biomedical engineering at Catholic University of America and on the graduate faculty at the University of Maryland Medical School.